Applied Surface Science 495 (2019) 143544

Contents lists available at ScienceDirect

Applied Surface Science

journal homepage: www.elsevier.com/locate/apsusc

Full length article

# Polycrystalline 1-D TiN-based free-standing composite electrode for high performance of Li-polysulfide cells

Anteneh Marelign Beyene[1,2], Jong Hyuk Yun[1], Syed Abdul Ahad, Brindha Moorthy, Do Kyung Kim*

*Department of Materials Science and Engineering, KAIST, Yuseong-gu, Daejeon 34141, Republic of Korea*

ARTICLE INFO

*Keywords:*
Lithium-sulfur batteries
Titanium nitride
Polar host
Free-standing electrode

ABSTRACT

Li-sulfur batteries are expected to transform electrochemical energy storage technology by taking it to the next level, as it holds the possibility to obtain a higher energy density levels than state-of-the-art Li-ion batteries. The poor electrical conductivity of sulfur and the high diffusivity of the intermediate lithium polysulfides create various problems, which limit the utilization of the full potential of these batteries. Polar conductive sulfur hosts such as titanium nitride (TiN) make it possible to realize remarkable improvements in active material utilization and capacity retention outcomes over long-term cycling. It has not been possible to use these polar, conductive, ceramic materials for higher active material loading ($> 2\,mg\,cm^{-2}$) due to their low flexibility compared to carbonaceous materials. Here, we demonstrate the possibility of designing a three-dimensional free-standing electrode using polycrystalline 1-D TiN for a relatively high sulfur loading of $2.5\,mg\,cm^{-2}$. The electrochemical performance of this 1-D TiN-based electrode is compared to that of an electrode based on 1-D $TiO_2$ (the starting material for TiN synthesis). The results demonstrate the catalytic effect of TiN by virtue of its endowed conductivity, leading to remarkable capacity retention and better active material utilization at high C-rates compared to a $TiO_2$-based electrode.

## 1. Introduction

Li-sulfur batteries are among the promising candidates under investigation to meet the demand for next-generation energy storage [1–5]. The high abundance of sulfur, its relative low mass and its ability to adopt wide variety of oxidation states make Li—S batteries among the most promising candidates as low-cost and high-energy-density batteries [6–11]. Nevertheless, there are challenges which hinder the realization of Li—S batteries to their full potential. The fundamental challenges in the Li—S system are the highly insulating nature of sulfur and lithium sulfides, polysulfide dissolution in the electrolyte and the consequent shuttling problem, high volume expansion at the cathode, and dendrite formation at the anode [6,12–15]. The aforementioned problems are aggravated when high sulfur loading is employed at the cathode. A large number of investigations have been carried out to alleviate these problems since sulfur was initially used as cathode in the Li—S battery system. The majority of Li—S studies have focused on the cathode part, although there have also been studies of the anode, separator, and the electrolyte too [16].

Earlier reports focus on using different carbon nanostructures to make a carbon-sulfur composite cathode in order to realize a conductive network in a composite cathode and physically entrap polysulfides [17–19]. It is possible to achieve remarkable performance improvements by employing different carbon nanostructures with different cathode architectures [20]. However, the physical entrapment in these cases was not strong enough to hold the polysulfides during long-term cycling. Eventually, the polysulfides dissolve into the electrolyte and migrate to the anode, leading to active material loss, accumulation of the insulating layer at the anode, and ultimately capacity fading. Chemical entrapment of polysulfides using multifunctional cathodes was the next level of advancement in the development of Li—S battery cathodes [14]. Numerous studies have demonstrated the effectiveness of chemically binding polysulfides for long-term cycling by employing different surface-functionalized and/or polar sulfur hosts [21]. Carbonaceous materials, such as rGO, functionalized rGO, nitrogen-doped graphene, and graphitic carbon nitride (g-$C_3N_4$), possessing some degree of induced polarity, were among the first to be used as polar sulfur hosts due to their good conductivity levels. However, as the

* Corresponding author.
*E-mail address:* dkkim@kaist.ac.kr (D.K. Kim).
[1] These authors contributed equally.
[2] Permanent address: School of Chemical and Bioengineering, Addis Ababa Institute of Technology (AAiT), King George VI St., Addis Ababa 1000, Ethiopia.

https://doi.org/10.1016/j.apsusc.2019.143544
Received 16 April 2019; Received in revised form 10 July 2019; Accepted 30 July 2019
Available online 03 August 2019
0169-4332/ 

amount of oxygen or nitrogen in the carbon structure is increased, the conductivity is usually compromised, which limits further development of these materials [14]. Moreover, carbonaceous materials require large quantities of electrolytes (> 40 wt% of the electrode) to wet their large surface areas. However, this reduces the volumetric energy density of the cell and deteriorates the polysulfide dissolution problem. Consequently, the need arises to look beyond carbonaceous materials as Li—S host materials. In relation to this, metal oxides, which are well-known polar compounds, have been considered as alternatives. Oxides such as $SiO_2$, $MnO_2$ and $TiO_2$ have been investigate as sulfur hosts and as additives in carbon sulfur composite cathodes in the Li—S battery system [22,23] and have demonstrated good performances. However, due to their poor electronic conductivity, they could not be a complete remedy to the problem. They are efficient in terms of immobilizing lithium polysulfides thereby preventing the shuttling mechanism, but they still require the presence of a large quantity of carbon to facilitate electron transfer in the system.

Recently, sub-oxides (such as $Ti_4O_7$) [24], nitrides (e.g., TiN) [25], carbides (TiC) [26] and sulfides (e.g., $SnS_2$) [27] have received attention in relation to Li-sulfur batteries, as these materials are both highly electrically conductive and polar materials. Some reports demonstrate that these polar conductive materials enhance the reversible conversion of sulfur to $Li_2S$ by effectively immobilizing the polysulfides and catalyzing the electrochemical redox reaction through the ready provision of necessary electrons for the reaction [26,28]. It is possible to achieve remarkable electrochemical performance outcomes using such polar conductive materials; nevertheless, nearly all published performances were obtained using the traditional slurry casting method of the electrode design, in which the sulfur loading level is usually low ($< 2\ mg\ cm^{-2}$). Currently, it is well recognized that with sulfur loading levels of $< 2\ mg\ cm^{-2}$, it is difficult to achieve the high energy density (500–600 $Wh\ kg^{-1}$) anticipated by researchers. Attempts to increase the mass loading using the slurry-casting method usually encounter several problems, such as delamination of the active material from the current collector and poor contact between the sulfur, electrolyte, and conductive carbon. Another issue is excessive polysulfide dissolution.

The three-dimensional free-standing electrode design has been found to be viable option to avoid the problems associated with high sulfur loading in slurry-casted electrode designs. Several reports have demonstrated high sulfur loading ($> 60\ mg\ cm^{-2}$) [29] with reasonable performance using different sulfur/polysulfide-infiltrated carbon nanostructures [13,30,31]. With this approach, it is possible to achieve higher power density and higher areal capacity levels (up to $56\ mAh\ cm^{-2}$) [29]. However, because most of the materials used to construct these three-dimensional free-standing electrodes are based on carbon, the inherently poor polysulfide-trapping ability of carbon inevitably limits their long-term cycleability. Recently, our group reported a glass-fiber-based polysulfide-infiltrated free-standing electrode in an attempt to realize significant reductions in the amount of carbon [20]. It was an excellent design, which used glass fiber (polar material) as a polysulfide reservoir with a small amount of CNT for conductivity and a small amount of $MnO_2$ for enhanced polysulfide immobilization. It was possible to realize outstanding performance at a higher sulfur loading of $5\ mg\ cm^{-2}$.

In the present work, we demonstrate the use of one-dimensional (1-D) TiN alone to construct a three-dimensional free-standing electrode while avoiding the need to use expensive CNT for conductivity and $MnO_2$ for polysulfide immobilization. It was possible to demonstrate promising performance with a sulfur loading of $2.5\ mg\ cm^{-2}$. Several reports have demonstrated the use of 1-D TiN as a sulfur host in Li-sulfur batteries typically using a slurry-casting electrode design approach with sulfur loading of $< 2\ mg\ cm^{-2}$ [28,32–34]. To the best of our knowledge, this is the first attempt to use 1-D TiN for a free-standing electrode deign with a relatively higher sulfur loading.

## 2. Experimental

### 2.1. Material synthesis and characterization

A process of carbothermal reduction followed by the nitridation of 1-D rutile $TiO_2$ (pre-synthesized using the molten salt synthesis method [36]) was utilized to synthesize polycrystalline 1-D TiN. Melamine ($C_3H_6N_6$) (99%, Sigma Aldrich), which is composed of 66% nitrogen by weight, was used as a reducing agent and as a nitrogen source. The synthesis technique adopted here is from a previous report; it is facile and avoids the use of flammable $NH_3$ gas. An $N_2$ atmosphere served as both an inert atmosphere and as a supplementary $N_2$ source for the reaction. The 1-D rutile $TiO_2$ was thoroughly mixed with a greater quantity (fivefold by weight) of melamine using a mortar and pestle. The mixed powder was formed into a pellet using a low-pressure isostatic press to make it convenient for handling. The formed pellet was then transferred to a tube furnace, where it underwent a two-stage heat treatment under a nitrogen atmosphere. The heat treatment was done at 400 °C for 3 h and then at 900 °C for 6 h, where both the heating and cooling rates were 5 °C/min. After the heat treatment, the resulting pellet was grounded into a powder to prepare it for the analysis.

The morphology of the synthesized powder was analyzed using a field-emission scanning electron microscope (FE-SEM; XL 30, Philips, Netherlands), and its phase was analyzed using high-resolution X-ray diffraction (XRD; Rigaku D/Max-RB, 12 KW, Japan) with Cu Kα radiation ($\lambda = 1.5148$ Å) operating at 40 kV and 300 mA. The TG-DSC analysis was done using a thermogravimetric analysis and differential scanning calorimetry, with the precursor powder mixture, from room temperature to the synthesis temperature. High-resolution TEM (HR-TEM) and SAD analyses were carried out using a transmission electron microscope (TEM; Model Tecnai G2 F30 S-Twin, FEI, Eindhoven, The Netherlands) with an acceleration voltage of 300 kV. The chemical bonding was analyzed by X-ray photoelectron spectroscopy (XPS, Thermo VG Scientific). A polysulfide trapping ability test was conducted by preparing $Li_2S_8$ solution in DOL/DME (50:50 by volume) as a solvent with equal amounts of the TiN, $TiO_2$, and Super P powders.

### 2.2. Polysulfide-impregnated free-standing electrode preparation method

To fabricate the free-standing electrode, 90 wt% 1-D polycrystalline TiN, 10 wt% conducting carbon Super P (Timcal), and a few drops of PTFE binder and isopropyl alcohol (IPA) as a solvent were used. The 1-D TiN powder was thoroughly mixed with the conducting carbon Super P using a mortar and pestle. A few drops of the PTFE binder suspension were added to the top of the well-mixed 1-D TiN/carbon powder mixture, which was further ground for several minutes while simultaneously adding isopropyl alcohol (IPA) as a solvent dropwise until a thick paste with good consistency had formed. The thick paste was then made into a sheet using a roller and a flat surface. Discs with a dimeter of 12 mm were punched out of the sheet and were then put in a vacuum oven at 60 °C overnight to evaporate the solvent. A solvent-free electrode was thus obtained. For polysulfide impregnation, a 0.5 M $Li_2S_8$ solution in DOL/DME (1:1 volume ratio) was initially prepared. Subsequently, 22.1 µl of the prepared solution, which corresponds to an areal sulfur loading of $2.5\ mg\ cm^{-2}$, was impregnated into the free-standing electrode. The control samples of 1-D $TiO_2$-based, and commercial bulk TiN (< 3 µm, Sigma Aldrich) based electrodes were fabricated along the same method.

### 2.3. Cell assembly and electrochemical measurements

Electrochemical measurements of all electrodes were taken by preparing 2032-type coin cells, which were assembled in an Ar-filled glove box. The polysulfide-impregnated free-standing electrode and lithium foil were used as the working and counter/reference electrodes, respectively. The electrolyte was prepared by dissolving 1 M lithium bis

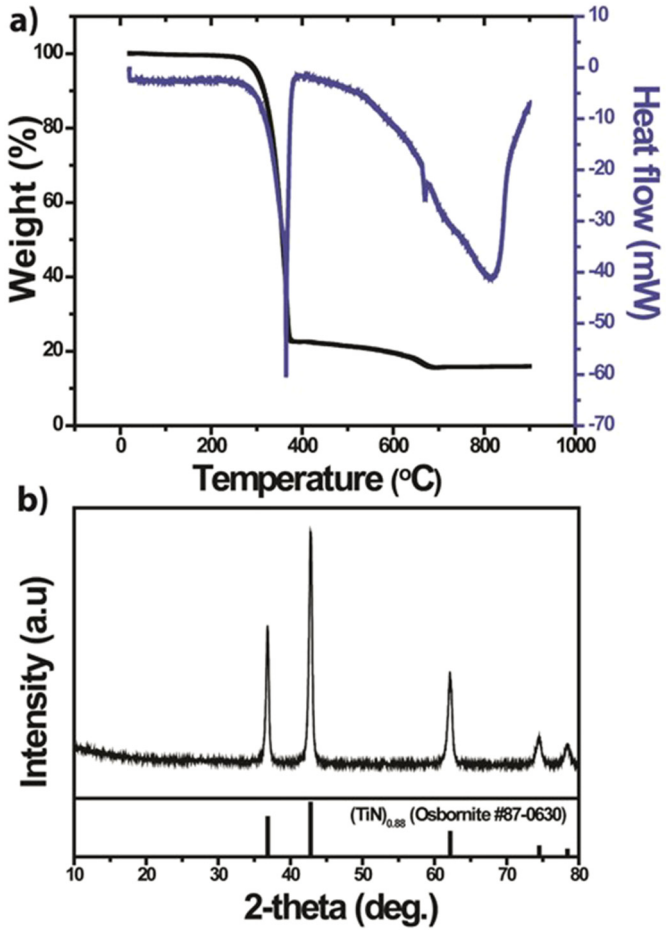


**Fig. 1.** a) TG-DSC analysis of the $TiO_2$/melamine powder mixture from room temperature to 900 °C, and b) XRD pattern of the synthesized powder and the standard JCPDS # 87-0630 pattern.

(trifluoromethanesulfonyl)imide (LiTFSI) (Sigma Aldrich) and 0.2 M lithium nitrate (Sigma Aldrich) in solvents of 1,3-dioxolane (anhydrous, contains ~75 ppm BHT as an inhibitor, 99.8%, Sigma-Aldrich) and 1,2-dimethoxyethane (anhydrous, 99.5%, Sigma-Aldrich) (1:1 volume ratio). Before the electrolyte preparation step, these solvents were stored over molecular sieves for 24 h to remove moisture. Polypropylene membranes (Celgard, Inc.) were used as separators. Galvanostatic measurements were taken in the potential range of 1.7 to 2.8 V vs. $Li^+$/Li using a battery cycler (WBCS3000, WonATech). The C-rates for all coin cells were calculated based on the theoretical capacity of sulfur in the composite, for which the 1 C rate is 1672 mA $g^{-1}$. All electrochemical measurements were performed at room temperature.

## 3. Results and discussion

As indicated by the TG-DSC analysis (Fig. 1), ~78% of the total weight of the precursor mixture is lost at a temperature of ~360 °C with a corresponding endothermic peak in the DSC curve. According to the findings of a melamine decomposition analysis [35], around this temperature, the sublimation of melamine occurs. This fact justifies the need to use fivefold excess melamine by weight in the precursor powder mixture so that a small amount of melamine (~5 wt% of the total mixture) remains for an additional reaction. The melamine further undergoes a polycondensation reaction with the release of ammonia gas at around 670 °C, which can initiate an earlier reduction of 1-D $TiO_2$ to some extent. At around 815 °C, the complete decomposition of the polycondensed product occurs and consequently the carbothermal reduction and nitridation reactions proceed further. The nitration reaction is supplemented by the surrounding $N_2$ atmosphere in addition to the ammonia (the decomposition product).

Phase identification and purity checks and a structural analysis of the synthesized powder were carried out. The phase identification and purity check were done by means of an X-ray diffraction analysis. As presented in Fig. 1b, the diffraction patterns of the powder match precisely the standard reference pattern of 1-D TiN (JCPDS # 87-0630), indicating the formation of the anticipated pure TiN phase. To check the morphology of the powder, scanning electron microscopy (SEM) and transmission electron microscopic (TEM) analyses were conducted. The SEM analysis (Fig. 2d) reveals that the powder is composed of 1-D structures with an average length ~2.5 μm and an average thickness ~400 nm. The average length of the synthesized powder is shorter and its average width is also thicker than the starting 1-D rutile $TiO_2$ (average length ~5 μm and average thickness ~340 nm) [36]; most likely, the longer rods break during the high-temperature heat treatment, with a consequent structural change following the formation of a new phase. The TEM micrograph (Fig. 2a) clarifies that the 1-D structure is a rod (not a hollow structure) and that it has a rough surface. The HRTEM and SAED patterns (Fig. 2b and c) indicate the polycrystallinity of the powder. As described in the HRTEM image, the grain size of the 1-D polycrystalline rod is ~10 nm. The d spacing of a single grain corresponds to the (111) crystallographic surface of TiN, which is in agreement with the XRD analysis result. The ring pattern of the SAD analysis reveals that the particles are polycrystalline, and the indexing of each ring pattern is consistent with the diffraction peaks of the XRD analysis, further confirming the formation of the TiN phase.

The pure-phase, 1-D, polycrystalline TiN powder was used to fabricate the free-standing electrode. For comparison, a free-standing electrode of the same type was also created from the starting 1-D rutile $TiO_2$, and commercial bulk TiN (particle size < 3 μm). The 1-D $TiO_2$-based electrode was fabricated to be compared with 1-D TiN on the electrical conductivity and polysulfide chemisorption ability. The commercial bulk TiN-based electrode was fabricated to be compared with 1-D TiN on the connectivity of particles affecting the path of charge carriers, because the spherical particles exhibit a large contact resistance and a poor particle connectivity than the one-dimensional particles. [31] Polysulfide infiltration (equivalent to sulfur loading of 2.5 mg $cm^{-2}$) was conducted with all electrodes, and electrochemical analyses were carried out after the fabrication of a coin cell using this polysulfide-infiltrated free-standing electrode as a cathode.

The electrochemical performance results are presented in Fig. 3. Fig. 3a presents the results of a CV analysis of the 1-D TiN-based, 1-D $TiO_2$-based, and the bulk TiN-based electrodes. All CV curves show the typical redox peaks of Li−S battery system. There are two reduction/cathodic peaks at around 2.3 V and 2.1 V, corresponding to the reduction of elemental sulfur ($S_8$) to the higher ($Li_2S_8$-$Li_2S_4$) and lower ($Li_2S_4$-$Li_2S_2$) order lithium polysulfide, respectively. An oxidation/anodic peak is also apparent at around 2.4 V, which corresponds to the oxidation of $Li_2S_2$/$Li_2S$ to higher-order Li-polysulfides and elemental sulfur. As indicated by the curves, the onset potentials of the redox peaks for all electrodes are comparable. Nevertheless, the reduction/cathodic peak potentials are shifted towards lower potentials while that of the oxidation/anodic peak potential is shifted towards a higher potential in the case of the 1-D $TiO_2$-based electrode compared to that of the 1-D TiN-based electrode. This indicates the two materials bind lithium polysulfides comparably well; however, the kinetics of the reduction reactions are faster in the case of the 1-D TiN-based electrode than that of the 1-D $TiO_2$-based electrode. An additional ~50 mV negative potential is needed to overcome the kinetic barrier in the case of the 1-D $TiO_2$-based electrode compared to 1-D TiN-based one. Similarly, the oxidation/anodic peak requires an additional ~30 mV positive potential to arise. The peak current values of the redox peaks are also higher for the 1-D TiN-based electrode compared to the 1-D $TiO_2$-based one, which is also additional proof of the faster reaction kinetics in the 1-D TiN-based electrode. For the bulk (spherical) TiN-based

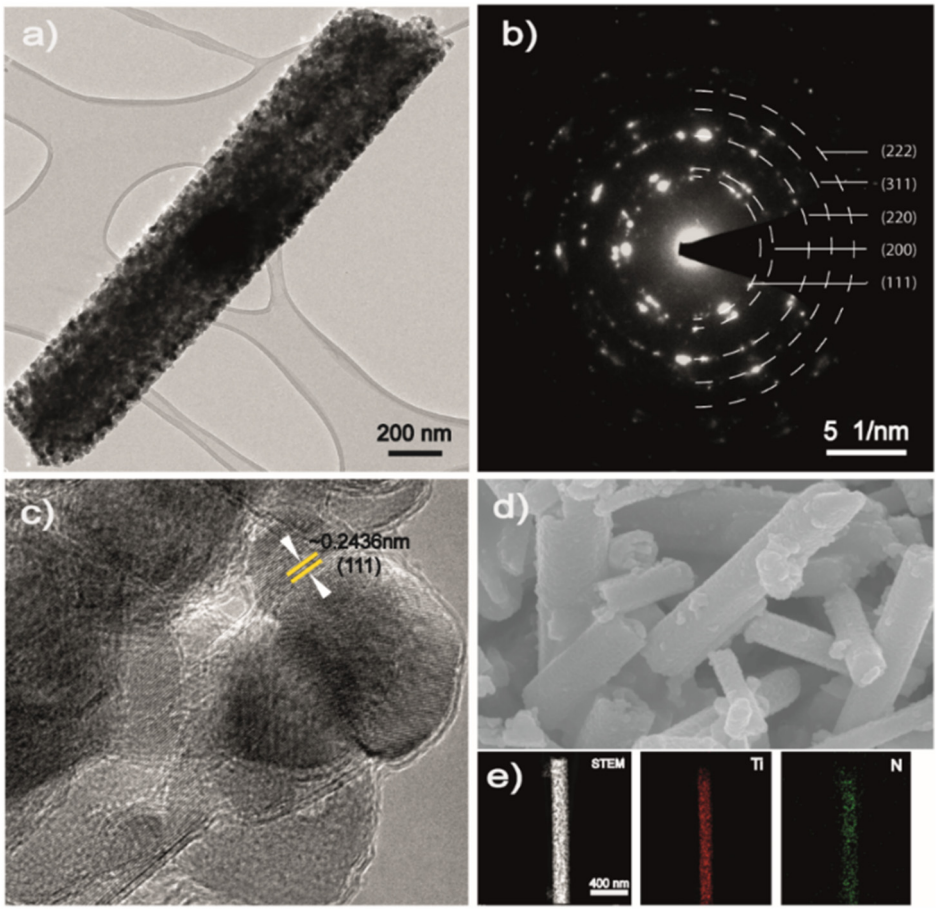


**Fig. 2.** a) TEM image, b) indexed SAD pattern, c) HRTEM image, d) SEM image, and e) STEM image and the corresponding elemental mapping of the synthesis product.

electrode, the peak current is much smaller at all voltage range than 1-D TiN and 1-D $TiO_2$ electrodes indicating the inferior diffusion of the charge carriers during charge/discharge. The cathodic peak related to the low order polysulfide transformation appears on a lower voltage under 2.0 V implying the polarization due to the charge transfer resistance from the poor connectivity compared to the 1-D materials.

The cycling performance outcomes of the three electrodes at a 0.1 C rate are presented in Fig. 3b. The first discharge capacity for the 1-D TiN-based electrode was 880 mAh $g^{-1}$ while that of the 1-D $TiO_2$-based electrode was 957 mAh $g^{-1}$, increasing to 1117 mAh $g^{-1}$ and 1135 mAh $g^{-1}$ respectively, during the second cycle. Because the first discharge starts at the OCV (~2.3 V) due to the $Li_2S_8$ in the Li-polysulfide batteries, instead of from elemental sulfur ($S_8$) as in the case of the common Li-sulfur system, the amount of charge which could have been released during the conversion from $S_8$ to $Li_2S_8$ does not contribute to the first discharge capacity. Consequently, the first discharge capacity in Li-polysulfide batteries is usually smaller, unlike in common Li-sulfur batteries. Starting with the second cycle, the charging/discharging behavior of the Li-polysulfide system becomes similar to that of a common Li-sulfur battery. The discharge capacity curve for the 1-D TiN electrode was highly stable for the first 20 cycles at around 1117 mAh $g^{-1}$, after which it starts to decline slowly, reaching 890 mAh $g^{-1}$ after 100 cycles. On the other hand, capacity decay occurs quickly in the 1-D $TiO_2$ electrode, from 1135 mAh $g^{-1}$ at the second cycle to 610 mAh $g^{-1}$ within 45 cycles. After the 45th cycle, the capacity decay becomes much more severe, with a capacity as low as ~190 mAh $g^{-1}$ during the next ten cycles. This significant difference in the discharge capacity curve is also a direct consequence of the enhanced kinetics obtained by virtue of the good conductivity of the 1-D TiN (unlike the highly insulative $TiO_2$) in addition to its good polysulfide binding ability. Polysulfide trapping occurs on the polar surfaces of 1-D TiN and 1-D $TiO_2$ particles in both composite electrodes. The polysulfides on the surface of 1-D TiN can easily convert from higher-order polysulfide to the lower-order type and then finally to $Li_2S$, as 1-D TiN allows the easy flow of necessary electrons for the consecutive sulfur reduction reactions. Consequently, the electrochemical redox reaction can occur smoothly on the surface of the 1-D TiN (owing to the catalytic effect of 1-D TiN due to its good conductivity), resulting in the remarkable capacity retention for several cycles. Nevertheless, 1-D $TiO_2$, which is not conductive in nature, can only trap polysulfides. The necessary electrons for the redox reaction can only be transferred through the 8% conductive carbon that composes the electrode. The polysulfides must be in contact with the conductive carbon for the necessary reduction reaction to occur to ensure a smooth charging/discharging process. There will be a higher probability that some of the polysulfides cannot obtain the necessary electrons and will thus remain trapped on the 1-D $TiO_2$ surface without undergoing a reversible reaction. This trapping of polysulfides without participation in the electrochemical reaction results in a loss of the active material and consequently quick capacity decay. In addition, the trapped polysulfides soon cover the entire surface of the 1-D $TiO_2$ particles, leading to a loss of the polysulfide trapping ability of the 1-D $TiO_2$ particles and resulting in further polysulfide shuttling and consequently severe capacity decay. In the case of the bulk TiN-based electrode, the specific discharge capacity is lower than the other electrodes in early stage in agreement with Fig. 3a, but retains effectively due to good polysulfide chemisorption ability of TiN.

The voltage-capacity curves shown in Fig. 3c and d provide further

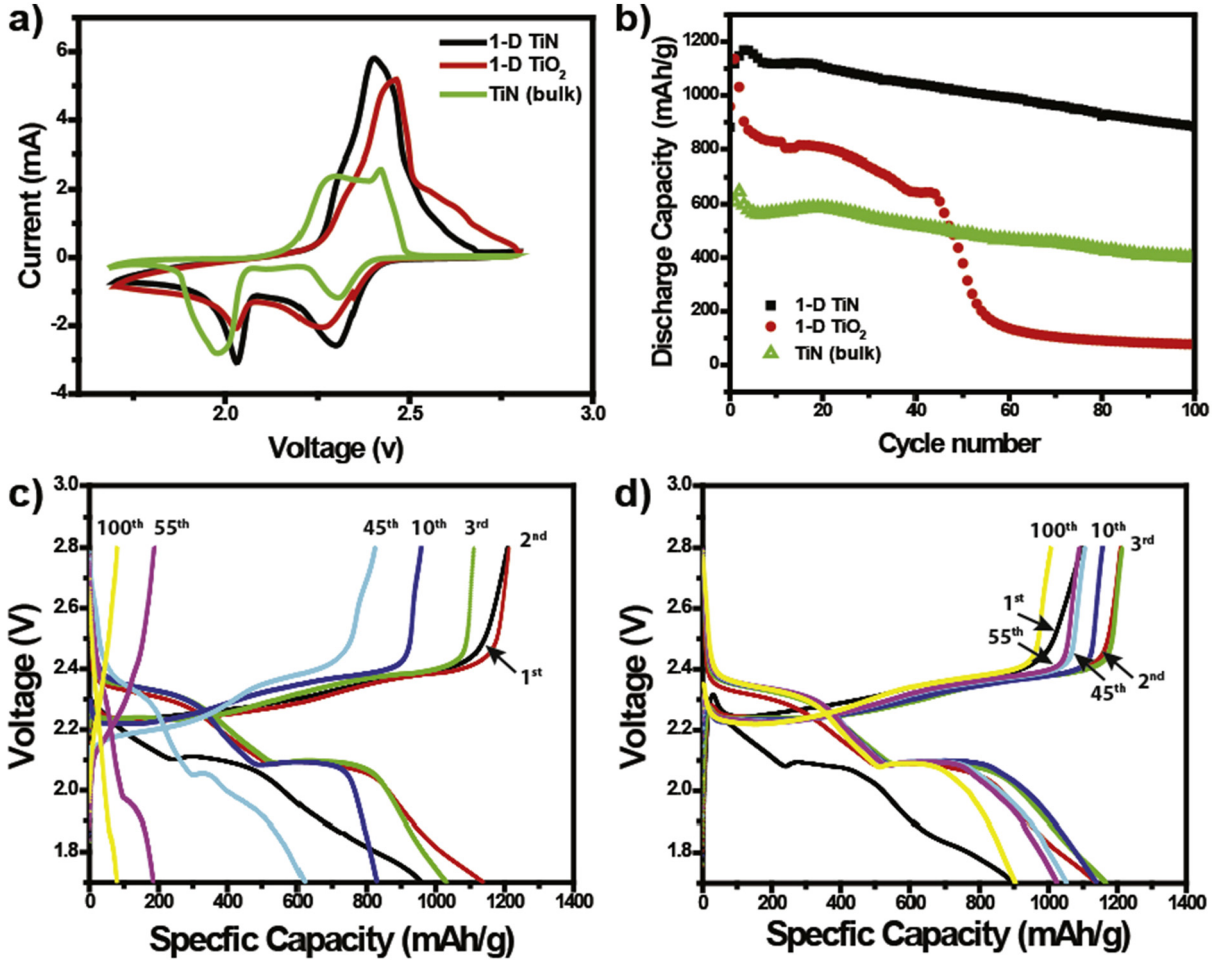


**Fig. 3.** a) CV analysis at 0.1 mV $s^{-1}$ scan rate, and b) discharge capacity for 100 cycles at the 0.1 C rate of polysulfide-infiltrated 1-D TiN-based, 1-D $TiO_2$-based, and commercial bulk TiN-based composite electrodes. The charge/discharge curves of c) polysulfide-infiltrated 1-D $TiO_2$-based composite electrode and d) the polysulfide-infiltrated 1-D TiN-based composite electrode.

insight into the charging/discharging behavior of the 1-D TiN and $TiO_2$ electrodes during cycling. The behaviors of the first cycles in the two electrodes are similar. A low discharge capacity is noted, with higher polarization than in the subsequent cycles and low columbic efficiency rates in both cases. Starting from the second up to the 100th cycle, the discharge curves show two typical plateaus of the electrochemical sulfur reduction reactions, indicating there were some active materials participating in the electrochemical reversible reaction up to the 100th cycle. Nevertheless, the amount of active materials participating in the electrochemical reaction and the charge transfer resistance within the two electrodes were not similar. For the electrode containing 1-D $TiO_2$, the second plateau for the discharge curve starts to decay significantly starting with the third cycle, which implies that the reduction reaction from the lower-order polysulfide ($Li_2S_4$ and $Li_2S_2$) to the final solid $Li_2S$ is not efficient in the system. This second reduction reaction, which accounts for three-fourths of the discharge capacity, involves a solid-solid reaction (from $Li_2S_2$ to $Li_2S$) where the reaction kinetics is low. The poor capability of $TiO_2$ particles to provide the necessary electrons readily for the reduction reaction aggravates the problem, causing only part of the active material to participate in the electrochemical reaction. The quick capacity decay is thus a direct consequence of the poor conductivity of the $TiO_2$ particles. The polarization between the charge/discharge curves also shows a drastic increment during cycling, indicating an increment of the charge transfer resistance in the composite electrode upon cycling. As discussed earlier, the surface of the $TiO_2$ particles could be covered with lithium polysulfides after several cycles. This can cause $TiO_2$ particles to lose their polysulfide trapping ability in subsequent cycles; consequently, the better opportunity to come into contact with the surrounding conductive carbon by being trapped on the surface of the $TiO_2$ particles will be lost, leading to high charge transfer resistance.

Unlike the case of the 1-D $TiO_2$-containing electrode, the second plateau of the voltage-capacity curve for 1-D TiN-containing electrode decays very slowly (Fig. 3d). The polarization between the charge and discharge curves also remains remarkably constant, even up to 100 cycles. The remarkably smooth and stable charge/discharge behavior observed in Fig. 3d is a clear manifestation of the benefit obtained from the catalytic effect of 1-D TiN particles by virtue of their good conductivity. The nature of the discharge capacity curve does not change up to the 100th cycle, although the second plateau is shortened. The polarization between the charge/discharge curves is also remarkably constant. These facts indicate that the catalytic ability of 1-D TiN was still feasible up to the 100th cycle. The slight capacity decay of this 1-D TiN-containing electrode with cycling may be due to the loss of some of the lower-order polysulfides (especially $Li_2S_2$) when they are physically trapped on the threads and interwoven structure created by the PTFE binder (which accounts for ~18% of the electrode), as indicated in Fig. 5a.

The superior performance of 1-D TiN over 1-D $TiO_2$, and bulk TiN becomes more apparent when charging/discharging is performed at higher rates. A thermogravimetric (TG) analysis of the electrodes (Fig. 4a) reveals that the 1-D TiN-based, 1-D rutile $TiO_2$-based, and bulk

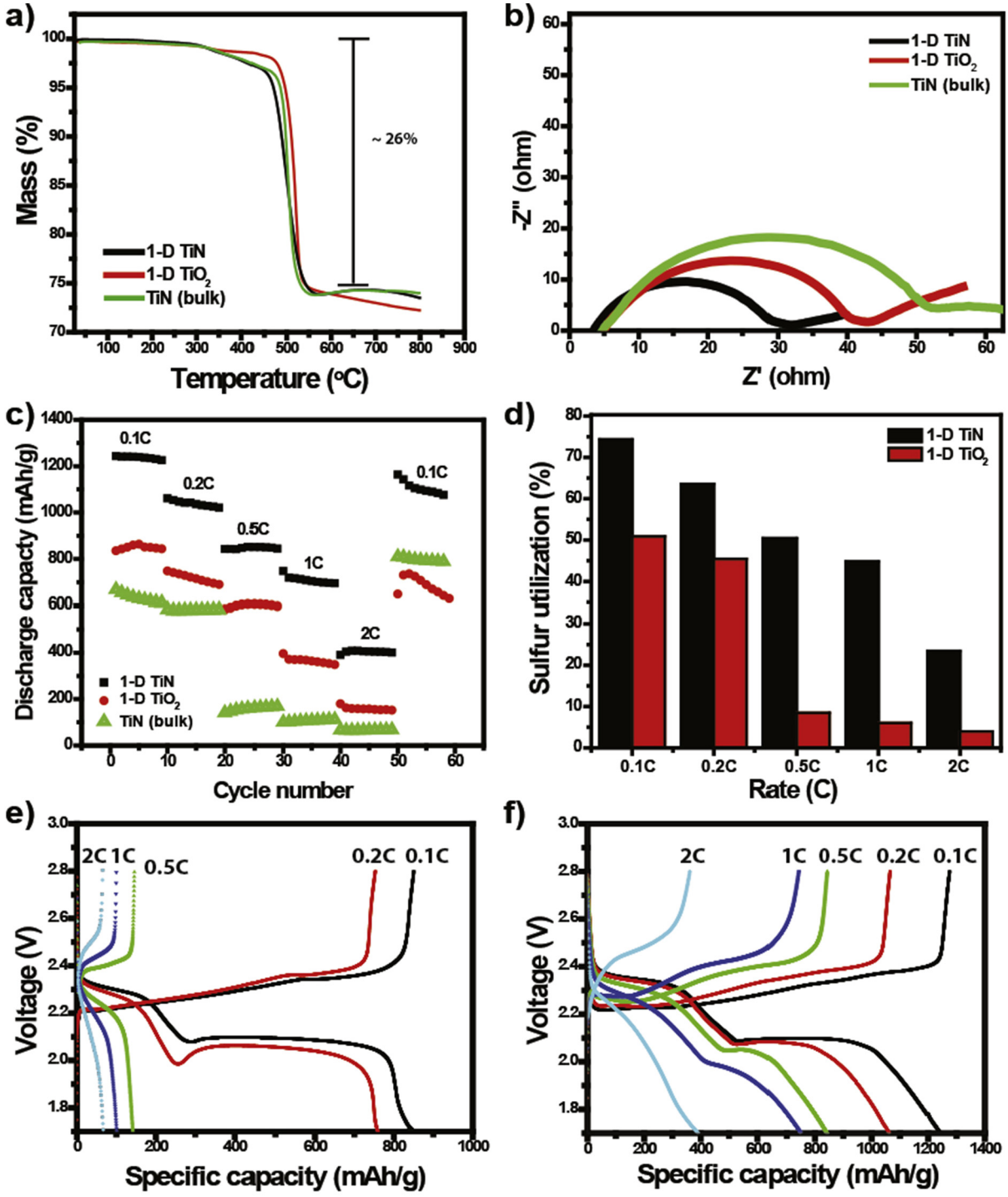


**Fig. 4.** a) Thermogravimetric (TG) analysis, b) electrochemical impedance spectroscopy (EIS) analysis, and c) rate capability of 1-D TiN-based, 1-D $TiO_2$-based, and commercial bulk TiN-based composite electrodes before polysulfide infiltration. d) Percent of active material utilization at different C-rates calculated using the first discharge capacity at each rate (the theoretical discharge capacity = 1672 mAh $g^{-1}$). The charge discharge curves of the first cycles at different C-rates for e) 1-D $TiO_2$ based composite electrode, and f) 1-D TiN based composite electrode.

TiN-based electrode are similarly composed of ~74% 1-D TiN/1-D $TiO_2$/TiN(bulk), ~18% PTFE binder, and ~8% super P. As shown in Fig. 4b, the charge transfer resistance is lower in the 1-D TiN-based electrode than in the 1-D $TiO_2$-based, and bulk TiN-based electrode. This result demonstrates that the TiN has higher electrical conductivity than $TiO_2$, and the 1-D particles exhibit a better particle connectivity than the bulk particles, which guarantees an excellent diffusion path of the electrons and lithium ions. This agrees with the following rate capability and Fig. 4c demonstrates the performance of the three electrodes at different C-rates. The gaps between the discharge capacity curves of the 1-D TiN-based and 1-D $TiO_2$-based electrodes become wider at higher rates (0.5 C, 1 C and 2 C) compared to those at lower rates (0.1 C and 0.2 C), indicating the superiority of the 1-D TiN-based electrode for high-rate cycling. The bulk TiN delivers a low discharge capacity at all C-rates due to large contact resistance. A quantitative analysis was conducted to clarify the enhanced kinetics in the case of the 1-D TiN-based electrode, which enables it to cope with rapid charge transfers at high rates. Fig. 4d shows clearly how the rate of active

material utilization drops to below 10%, from ~45% for the 1-D $TiO_2$-based electrode as the rate is increased from 0.2 C to 0.5 C. On the other hand, due to the enhanced reaction kinetics in the 1-D TiN-based electrode, active material utilization shows a normal progressive decline with an increase in the rate. Even at a 2 C rate, it was possible to obtain ~25% sulfur utilization. When the first discharge capacities of the 1-D $TiO_2$- and 1-D TiN-based electrodes at different C-rates (Fig. 4e and f) are analyzed, the 1-D $TiO_2$-based electrode shows a major step down in performance as the rate increases from 0.2 C to 0.5 C. This is also a clear indication of the poor charge transfer in the 1-D $TiO_2$-based electrodes. The rapidly moving electrons and ions return to their respective electrodes before interacting with a significant portion of the active material. Thus, only a very small portion of the active material has an opportunity to interact with the charges and undergo an electrochemical reaction.

It is clear from the theoretical understanding that the probability of the nonpolar conductive carbon to interact with polar lithium polysulfides is very low. However, a polysulfide-trapping experiment was conducted to investigate the further. A diluted $Li_2S_8$ solution (in 50 vol % DOL/DME solvent) was prepared. An equal volume of this solution was poured into four vials and 1-D TiN, Super P, and 1-D $TiO_2$ powders were mixed into three of them, leaving one as a blank control. A photographic image of the four vials after the mixed particles were settled and the results of a UV–Vis analysis of the corresponding supernatant solution are presented in Fig. 5b. The supernatant solution in the 1-D TiN- and 1-D $TiO_2$-containing vials appears transparent, whereas that containing super P appears to be identical to the blank control solution. The absorbance curve from the UV–Vis analysis also shows almost no absorbance in the visible range for the supernatant solutions from 1-D TiN and 1-D $TiO_2$, whereas that from super P indicates a curve similar to that of the blank solution. These experimental results clearly indicate how the polar TiN and $TiO_2$ can efficiently trap polysulfides, whereas the nonpolar super P barely interacts with the polysulfides. The surface area doesn't affect the UV–Vis analysis because the BET surface area of the 1-D TiN is similar to the 1-D $TiO_2$. The BET surface area of $TiO_2$ and TiN are 3.34 $m^2 g^{-1}$ and 4.33 $m^2 g^{-1}$, respectively. In both $TiO_2$ and TiN, the surface area is not large in the particle state, but after the free-standing electrode is formed, mesopore and macropore develop between particles and PTFE binder as shown in Fig. 5a. TiN has slightly larger specific surface area than that of $TiO_2$ but the difference is not that big as to make a significant impact on the electrochemical performance of the cells.

The UV–Vis analysis can be understood intuitively that without having much interaction with the polysulfides, the conductive carbon cannot contribute much to facilitate the necessary electron flow for a smooth, reversible electrochemical redox reaction. The conductive carbon only provides some conductivity for the 1-D $TiO_2$-containing electrode and to compensate for some degree of insulation introduced in the composite electrodes by the PTFE binder. XPS surface analysis results of the TiN-containing electrode before polysulfide impregnation (Fig. 6a) and of the polysulfide-impregnated TiN-containing electrode after 100 cycles (Fig. 6d) also confirm that 1-D TiN (not conductive carbon) is the material responsible for the good electrochemical reversible reaction by virtue of its strong interaction with the polysulfides and very good electronic conductivity. As shown in Fig. 6a and d, the nitrogen 1s spectra shift by ~2 eV towards the higher binding energy side for the polysulfide-impregnated sample (Fig. 6d) compared to the sample before the impregnation (Fig. 6a), which clearly indicates the strong interaction of the Li-polysulfides with 1-D TiN. On the other hand, the titanium 2p and carbon 1s (Fig. 6b, c, e & f) spectra scarcely show any change in the binding energy between the polysulfide-impregnated and non-impregnated electrodes, indicating that the interaction with the polysulfides occurs mostly by the nitrogen as compared to the titanium in the case of the TiN electrode. Regarding the conductive carbon, the result reveals that carbon undergoes very little or no interaction with the polysulfides, providing clear evidence of the superiority of the polar conductive TiN over conductive carbon-based electrodes.

## 4. Conclusion

The possibility of a three-dimensional, free-standing electrode design using 1-D TiN/$TiO_2$, PTFE as a binder, and small amount of a low-cost conductive carbon material (super P) was demonstrated. The electrochemical performance capabilities of free-standing electrodes infiltrated with a $Li_2S_8$ solution (equivalent to 2.5 mg $cm^{-2}$ sulfur loading) were tested. Both 1-D TiN-based and 1-D $TiO_2$-based electrodes demonstrated stable performance for several cycles; however, the 1-D TiN-based electrode demonstrated superiority in terms stable cycling for 100 cycles, remarkable rate capability, and much better active material utilization even at higher rates than the 1-D $TiO_2$ and bulk TiN. The superior performance of the 1-D TiN-based electrode is attributed to the enhanced reaction kinetics stemming from the excellent connectivity of 1-D environment and the catalytic behavior of TiN particles by virtue of their good conductivity. Polysulfide trapping tests and an XPS analysis further supported the benefit of the polar conductive 1-D TiN over the polar nonconductive 1-D $TiO_2$ and the nonpolar but conductive super P for enhanced performance. It paves way for the additional development of non-carbon-based free-standing electrode designs for high loading levels.

## Acknowledgement

This work was supported by the Climate Change Research Hub of EEWS from KAIST (Grant No. N11180108) and by a grant from the National Research Foundation of Korea (NRF) funded by the Korean

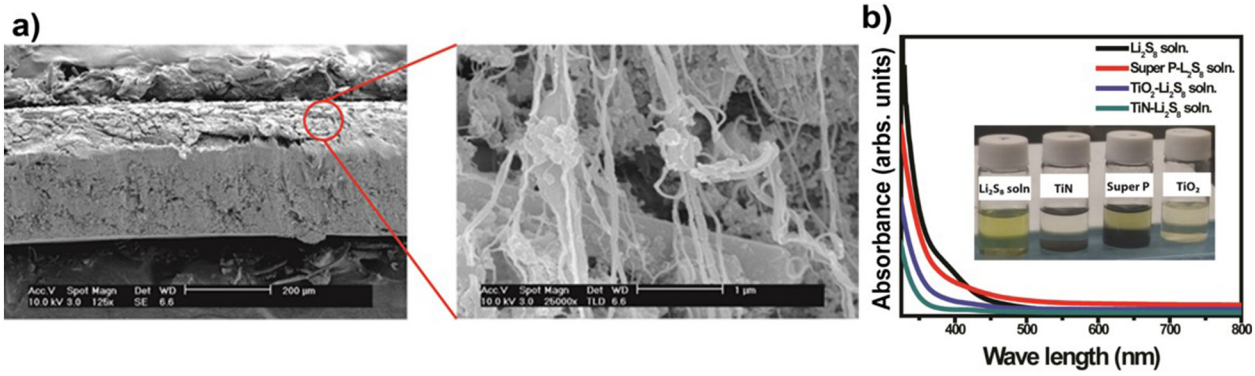


**Fig. 5.** a) Cross-sectional SEM image of the polysulfide infiltrated 1-D TiN based electrode after 100 cycles. b) UV–Vis analysis of the $Li_2S_8$ solution (in 50 vol% DOL/DME) and the supernatant solution obtained after the $Li_2S_8$ solution (in 50 vol% DOL/DME) is mixed with 1-D TiN, super P, and 1-D $TiO_2$ powder. The inset is a photographic image of the $Li_2S_8$ solution and the mixtures of the $Li_2S_8$ solution with 1-D TiN, super P, and 1-D $TiO_2$ powders.

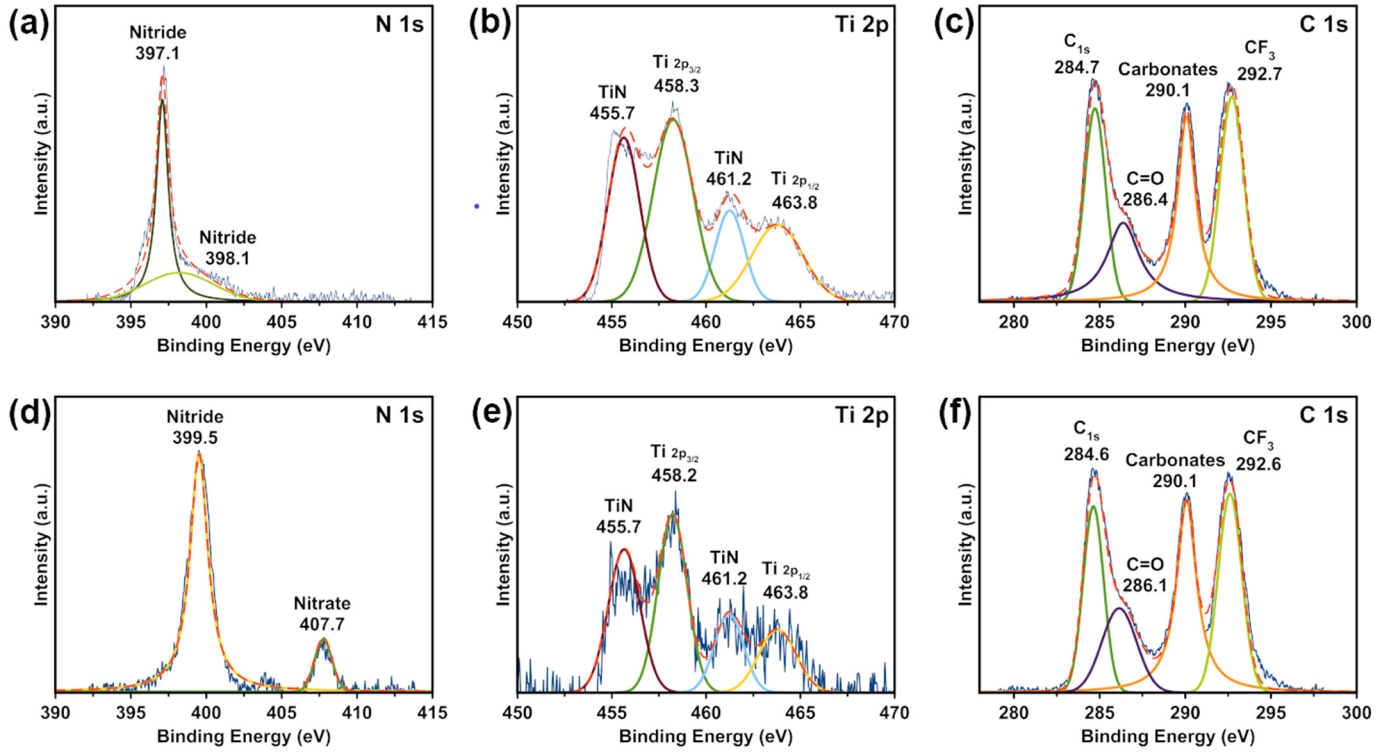


**Fig. 6.** XPS a) nitrogen 1s, b) titanium 2p, and c) carbon 1s spectra of the 1-D TiN-based composite electrodes before polysulfide infiltration; and d) nitrogen 1s, e) titanium 2p, and c) carbon 1s spectra of polysulfide-impregnated 1-D TiN-based composite electrode after 100 cycles.

government (MSIT) (No. 2017R1A2B2010148).

## References


[1] Y.B. An, Q.Z. Zhu, L.F. Hu, S.K. Yu, Q. Zhao, B. Xu, A hollow carbon foam with ultra-high sulfur loading for an integrated cathode of lithium-sulfur batteries, J. Mater. Chem. A 4 (2016) 15605–15611.

[2] B.D. McCloskey, Attainable gravimetric and volumetric energy density of Li-S and Li ion battery cells with solid separator-protected Li metal anodes, J. Phys. Chem. Lett. 6 (2015) 4581–4588.

[3] B. Scrosati, J. Garche, Lithium batteries: status, prospects and future, J. Power Sources 195 (2010) 2419–2430.

[4] M.Y. Li, R. Carter, A. Douglas, L. Oakes, C.L. Pint, Sulfur vapor-infiltrated 3D carbon nanotube foam for binder-free high areal capacity lithium-sulfur battery composite cathodes, ACS Nano 11 (2017) 4877–4884.

[5] A. Manthiram, Electrical energy storage: materials challenges and prospects, MRS Bull. 41 (2016) 624–630.

[6] W.M. Kang, N.P. Deng, J.G. Ju, Q.X. Li, D.Y. Wu, X.M. Ma, L. Li, M. Naebe, B.W. Cheng, A review of recent developments in rechargeable lithium-sulfur batteries, Nanoscale 8 (2016) 16541–16588.

[7] J.H. Yan, X.B. Liu, B.Y. Li, Capacity fade analysis of sulfur cathodes in lithium-sulfur batteries, Adv. Sci. 3 (2016) 1600101.

[8] R. Gopalakrishnan, S. Goutam, L.M. Oliveira, J.M. Timmermans, N. Omar, M. Messagie, P. Van den Bossche, J. van Mierlo, A comprehensive study on rechargeable energy storage technologies, J. Electrochem. Energy Convers. Storage 13 (2017) 40801.

[9] D. Deng, Li-ion batteries: basics, progress, and challenges, Energy Sci. Eng. 3 (2015) 385–418.

[10] H.J. Peng, J.Q. Huang, X.B. Cheng, Q. Zhang, Review on high-loading and high-energy lithium-sulfur batteries, Adv. Energy Mater. 7 (2017) 1700260.

[11] F.X. Wu, G. Yushin, Conversion cathodes for rechargeable lithium and lithium-ion batteries, Energy Environ. Sci. 10 (2017) 435–459.

[12] M.D. Patel, E. Cha, C. Kang, B. Gwalani, W. Choi, High performance rechargeable Li-S batteries using binder-free large sulfur-loaded three-dimensional carbon nanotubes, Carbon 118 (2017) 120–126.

[13] G.M. Zhou, E. Paek, G.S. Hwang, A. Manthiram, Long-life Li/polysulphide batteries with high sulphur loading enabled by lightweight three-dimensional nitrogen/sulphur-codoped graphene sponge, Nat. Commun. 6 (2015) 7760.

[14] Q. Pang, X. Liang, C.Y. Kwok, L.F. Nazar, Advances in lithium-sulfur batteries based on multifunctional cathodes and electrolytes, Nat. Energy 1 (2016) 16132.

[15] M. Barghamadi, A. Kapoor, C. Wen, A review on Li-S batteries as a high efficiency rechargeable lithium battery, J. Electrochem. Soc. 160 (2013) A1256–A1263.

[16] B. Moorthy, S. Kwon, J.H. Kim, P. Ragupathy, H.M. Lee, D.K. Kim, Tin sulfide modified separator as an efficient polysulfide trapper for stable cycling performance in Li-S batteries, Nanoscale Horiz. 4 (2019) 214–222.

[17] S. Moon, Y.H. Jung, W.K. Jung, D.S. Jung, J.W. Choi, D.K. Kim, Encapsulated monoclinic sulfur for stable cycling of Li-S rechargeable batteries, Adv. Mater. 25 (2013) 6547–6553.

[18] S. Moon, Y.H. Jung, D.K. Kim, Enhanced electrochemical performance of a cross-linked polyaniline-coated graphene oxide-sulfur composite for rechargeable lithium-sulfur batteries, J. Power Sources 294 (2015) 386–392.

[19] S. Moon, J.K. Yoo, Y.H. Jung, J.H. Kim, Y.S. Jung, D.K. Kim, Effective suppression of polysulfide dissolution by uniformly transfer-printed conducting polymer on sulfur cathode for Li-S batteries, J. Electrochem. Soc. 164 (2017) A6417–A6421.

[20] P. Ragupathy, S.A. Ahad, P.R. Kumar, H.W. Lee, D.K. Kim, A flexible glass fiber based free-standing composite electrode for high-performance lithium polysulfide batteries, Advanced Sustainable Systems 1 (2017) 1700083.

[21] S.A. Ahad, P.R. Kumar, J.H. Kim, D.J. Kim, P. Ragupathy, D.K. Kim, Catecholamine-functionalized reduced graphene oxide: a scalable carbon host for stable cycling in lithium-sulfur batteries, Electrochim. Acta 246 (2017) 451–458.

[22] K.Y. Xie, Y.Z. Han, W.F. Wei, H.R. Yu, C.B. Zhang, J.G. Wang, W. Lu, B.Q. Wei, Fabrication of a novel $TiO_2$/S composite cathode for high performance lithium-sulfur batteries, RSC Adv. 5 (2015) 77348–77353.

[23] S.A. Ahad, P. Ragupathy, S. Ryu, H.W. Lee, D.K. Kim, Unveiling the synergistic effect of polysulfide additive and $MnO_2$ hollow spheres in evolving a stable cyclic performance in Li-S batteries, Chem. Commun. 53 (2017) 8782–8785.

[24] Q. Pang, D. Kundu, M. Cuisinier, L.F. Nazar, Surface-enhanced redox chemistry of polysulphides on a metallic and polar host for lithium-sulphur batteries, Nat. Commun. 5 (2014).

[25] N. Mosavati, V.R. Chitturi, S.O. Salley, K.Y.S. Ng, Nanostructured titanium nitride as a novel cathode for high performance lithium/dissolved polysulfide batteries, J. Power Sources 321 (2016) 87–93.

[26] H.J. Peng, G. Zhang, X. Chen, Z.W. Zhang, W.T. Xu, J.Q. Huang, Q. Zhang, Enhanced electrochemical kinetics on conductive polar mediators for lithium-sulfur batteries, Angew. Chem. Int. Ed. 55 (2016) 12990–12995.

[27] G.M. Zhou, H.Z. Tian, Y. Jin, X.Y. Tao, B.F. Liu, R.F. Zhang, Z.W. Seh, D. Zhuo, Y.Y. Liu, J. Sun, J. Zhao, C.X. Zu, D.S. Wu, Q.F. Zhang, Y. Cui, Catalytic oxidation of $Li_2S$ on the surface of metal sulfides for Li-S batteries, Proc. Natl. Acad. Sci. USA 114 (2017) 840–845.

[28] T.G. Jeong, D.S. Choi, H. Song, J. Choi, S.A. Park, S.H. Oh, H. Kim, Y. Jung, Y.T. Kim, Heterogeneous catalysis for lithium-sulfur batteries: enhanced rate performance by promoting polysulfide fragmentations, ACS Energy Lett. 2 (2017) 327–333.

[29] S.H. Chung, C.H. Chang, A. Manthiram, A carbon-cotton cathode with ultrahigh-loading capability for statically and dynamically stable lithium-sulfur batteries, ACS Nano 10 (2016) 10462–10470.

[30] Y.W. Ma, H.Z. Zhang, B.S. Wu, M.R. Wang, X.F. Li, H.M. Zhang, Lithium sulfur primary battery with super high energy density: based on the cauliflower-like structured C/S cathode, Sci. Rep. 5 (2015) 14949.

[31] J.H. Yun, J.H. Kim, D.K. Kim, H.W. Lee, Suppressing polysulfide dissolution via cohesive forces by interwoven carbon nanofibers for high-areal-capacity lithium-

sulfur batteries, Nano Lett. 18 (2018) 475–481.
[32] Z.M. Cui, C.X. Zu, W.D. Zhou, A. Manthiram, J.B. Goodenough, Mesoporous titanium nitride-enabled highly stable lithium-sulfur batteries, Adv. Mater. 28 (2016) 6926–6931.
[33] D.R. Deng, T.H. An, Y.J. Li, Q.H. Wu, M.S. Zheng, Q.F. Dong, Hollow porous titanium nitride tubes as a cathode electrode for extremely stable Li-S batteries, J. Mater. Chem. A 4 (2016) 16184–16190.
[34] Z.X. Hao, L.X. Yuan, C.J. Chen, J.W. Xiang, Y.Y. Li, Z.M. Huang, P. Hu, Y.H. Huang, TiN as a simple and efficient polysulfide immobilizer for lithium-sulfur batteries, J. Mater. Chem. A 4 (2016) 17711–17717.
[35] L. Costa, G. Camino, Thermal-behavior of melamine, J. Therm. Anal. 34 (1988) 423–429.
[36] A.M. Beyene, C. Baek, W.K. Jung, P. Ragupathy, D.K. Kim, Understanding the role of oxygen ion ($O_2^-$) activity in 1-D crystal growth of rutile $TiO_2$ in molten salts, CrystEngComm 20 (2018) 487–495.